Influence of pre-scission neutron emission on high-energy ^{238}U fission studied by the Langevin approach

Yingge Huang (黄英格), Yujie Feng (冯玉洁), Erxi Xiao (肖尔熙), Xin Lei (雷昕), Long Zhu (祝龙), and Jun Su (苏军)*
Sino-French Institute of Nuclear Engineering and Technology, Sun Yat-sen University, Zhuhai 519082, China

(Received 6 August 2022; accepted 26 October 2022; published 16 November 2022)

Background: The information about the pre-scission emitted neutrons is crucial for the fission dynamics study such as fission time scale and dissipation mechanism.
Purpose: The aim is to investigate the influence of the pre-scission neutron emission on the fragments mass, total kinetic energy, and the deformation distribution at the scission point in $^{238}\mathrm{U}(n, f)$ fissions at 110, 325, and 500 MeV.
Method: A three-dimensional Langevin approach considering nucleus elongation, deformation, and mass asymmetry is applied to simulate fission dynamics. The Hauser-Feshbach statistical decay model is coupled to simulate the pre-scission neutron emission.
Results: The properties of the pre-scission emitted neutron are first investigated. It is found that the multiplicity and the average kinetic energy increase with increasing excitation energy. The energy carried away by neutron emission is not negligible and it leads to the multichance fission, especially for the 110 MeV case. The fragments mass, total kinetic energy, and the deformation distribution at the scission point are then calculated with and without coupling the Hauser-Feshbach statistical decay model. It is found that the calculations partially reproduce the leftward shift of the experimental fragment mass distribution at high excitation energy. The pre-scission neutron emission also causes a reduction of the average total kinetic energy by about 2 MeV and a leftward shift of the distribution. The deformation distribution shows that about 75% of the fragments are produced in spherical and prolate ellipsoid shapes. No significant influence on deformation at the scission point was found.
Conclusions: For high-energy fission, the energy reduction by pre-scission neutron emission should be considered, which will lead to the multichance fission. The pre-scission neutron emission is one of the reasons for the decrease of the average mass and the leftward shift of the fission fragments mass and total kinetic energy distribution.

DOI: 10.1103/PhysRevC.106.054606

I. INTRODUCTION

Nuclear fission has been extensively studied since its discovery in 1938, but the comprehensive explanation of the fission mechanism is still not available. The mechanism about pre-scission neutron emission is one aspect that is not fully understood. It is one of the most effective probe to study the nuclear dissipation [1–7], fission time scale [8–11], nuclear level density [12,13], and nuclear temperature [14,15], because of the good distinguishability in experiment. Experimentally, a strong excitation energy dependence is found in fission fragment mass distribution. This property is mainly shown as the change of the fission mode and the average mass reduction of the fragments [16]. For the latter, one has suggested that the mechanism is related to the pre-scission neutron emission [17]. On the other hand, the multiplicity of prompt and delayed neutrons are two key data in reactor physics that correlate with the fission fragment excitation energy. However, the energy of the compound nucleus is carried away by pre-scission emitted neutrons, thus the nascent fragment excitation energy reduces. This will affect the prediction of prompt and delayed neutrons multiplicity in reactor design.

As a common theoretical method, the Langevin approach has been widely used in the study of the nuclear fission dynamics. Considering the nuclear collective motion, the Langevin model regards the fission process as a Brownian motion in the fission potential energy space. The dissipative and fluctuating phenomena in fission can be successfully reproduced. Establishing more connections to the micro-framework and other theoretical approach is the developing direction of Langevin approach [18], for example, the microscopic effects in the calculation of mass and friction tensors [19–21] and the neutron multiplicity mechanism [2,22–26].

In this work, the three-dimensional Langevin approach is developed by coupling the Hauser-Feshbach statistical decay model, and then applied to study the pre-scission neutron emission and its influence on the fragment mass, total kinetic energy and deformation in high energy induced $^{238}\mathrm{U}(n, f)$. This paper is organized as follows. In Sec. II, we present the detail of theoretical model. In Sec. III, the simulation results as well as some discussions are given. In Sec. IV, a summary of our work are presented.

*sujun3@mail.sysu.edu.cn

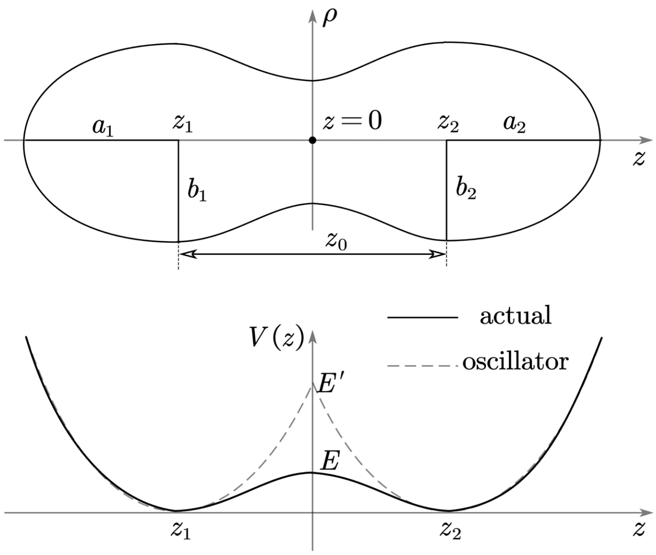

FIG. 1. The nuclear shape description in the two-center shell model (top) and the corresponding actual potential (bottom).

II. THEORETICAL FRAMEWORK

A. Nuclear shape parametrization

Fission is a large scale deformation motion of the nucleus. How to describe the shape of the nucleus during the reaction is a key part in the fission study. In this work, the nuclear shape description in the two center shell model (TCSM) [27] is used. The shape expression in the cylindrical coordinate is

$$\rho_s^2 = \begin{cases} b_1^2\left(1-\frac{z_1'^2}{a_1^2}\right) & z < z_1, \\ b_1^2\left(1-\frac{z_1'^2}{a_1^2}\left(1+c_1 z_1' + d_1 z_1'^2\right)\right)/\left(1+g_1 z_1'^2\right) & z_1 \leqslant z < 0, \\ b_2^2\left(1-\frac{z_2'^2}{a_2^2}\left(1+c_2 z_2' + d_2 z_2'^2\right)\right)/\left(1+g_2 z_2'^2\right) & 0 \leqslant z < z_2, \\ b_2^2\left(1-\frac{z_2'^2}{a_2^2}\right) & z_2 \leqslant z. \end{cases} \tag{1}$$

As shown in Fig. 1, $z_i' = z - z_i$, a_i and b_i are the short and long axes, the subscripts $i = 1, 2$ represent the two fission fragments. z_i is the fragment centers. One should note that z_i does not represent the position of mass center. The shape continuity conditions restrict the 12 variables in Eq. (1) to five, namely, the elongation of nucleus $z_0 = z_2 - z_1$, the mass asymmetry $\eta = (A_1 - A_2)/(A_1 + A_2)$, the deformation $\delta_i = (3\beta_i - 3)/(1 + 2\beta_i)$ with $\beta_i = a_i/b_i$, and the neck parameter ϵ. The neck parameter is defined as the ratio of the actual potential to the deformed oscillator potential along symmetry axis at $z = 0$, i.e., $\epsilon' = E/E'$ as shown in Fig. 1. For fission, ϵ' is suggested to be fixed at 0.35 [28], but it should not be considered that the neck radius is fixed. With additional constraint on deformation parameters $\delta_1 = \delta_2 = \delta$, nucleus deformation finally has three degrees of freedom $\{z_0/R_0, \delta, \eta\}$. $R_0 = r_0 A_{CN}^{1/3}$ denotes the radius of spherical compound nucleus and then the three parameters are all dimensionless.

In the TCSM nucleus shape description, the neck will be discontinuous when $\eta \neq 0$ and $z_0 = 0$. One solution proposed by Usang is to modify β_i as [19]

$$\begin{cases} \beta_1'(\delta, \eta) = \beta_1(1+\eta)f(z_0) + [1 - f(z_0)]\beta_1 \,, \\ \beta_2'(\delta, \eta) = \beta_2(1-\eta)f(z_0) + [1 - f(z_0)]\beta_2 \,, \end{cases} \tag{2}$$

where $f(z_0)$ is a transition function

$$f(z_0) = (1 + \exp[(z_0 - z_{00})/\Delta z_0])^{-1} \tag{3}$$

with $z_{00} = R_0$ and $\Delta z_0 = 0.2R_0$ two adjustable parameters.

B. The Langevin approach

The multidimensional Langevin equations are written as

$$\frac{dq_i}{dt} = (m^{-1})_{ij} p_j, \tag{4}$$

$$\frac{dp_i}{dt} = -\frac{\partial V}{\partial q_i} - \frac{1}{2}\frac{\partial (m^{-1})_{jk}}{\partial q_i} p_j p_k - \gamma_{ij}(m^{-1})_{jk} p_k + g_{ij}\Gamma_j(t), \tag{5}$$

where $\boldsymbol{q} = \{z_0/R_0, \delta, \eta\}$, $\boldsymbol{m}^{-1}$, $\boldsymbol{\gamma}$, and $\boldsymbol{g}$ correspond to the generalized coordinates, the inverse of the inertia tensor, the friction tensor, and the random force strength, respectively. $\boldsymbol{\Gamma}$ is the normalized Gaussian random force with average value 0. In Eqs. (4) and (5) and the following equations, the Einstein summation convention over equal pair indices is used. According to the fluctuation-dissipation theorem, the random force strength is related to the friction tensor, i.e.,

$$g_{ik} g_{jk} = \gamma_{ij} T^*, \tag{6}$$

where T^* is the effective nuclear temperature, which is related to the general nuclear temperature as follows [29]:

$$T^* = \frac{\hbar\bar{\omega}}{2} \coth \frac{\hbar\bar{\omega}}{2T} \tag{7}$$

with $\hbar\bar{\omega} = 2$ MeV [30]. According to the Fermi gas model, the nuclear temperature can be calculated by $E_{\text{int}} = a_n T^2$ with $a_n = A_{\text{CN}}/12$ is the level density parameter. E_{int} is the intrinsic excitation energy of compound nucleus related to total excitation energy E^*,

$$E_{\text{int}}(\boldsymbol{q}, t) = E^* - \sum \epsilon(t) - \sum B_{\text{pre}}(t) - \frac{1}{2}(m^{-1})_{ij} p_i p_j - V(\boldsymbol{q}, T = 0), \tag{8}$$

where ϵ and B_{pre} are the kinetic energy and the separation energy of pre-scission emitted particle, respectively. During the fission evolution, high excitation energy nucleus emits randomly light particles. And a part of E^* transfers into ϵ and B_{pre} when the emission happens. The first three terms at the right side of Eq. (8) show this permanent reduction of E^* by emitting pre-scission particles.

C. Potential energy

In the present work, the macro-microscopic model is considered in the calculation of fission potential energy. The total potential energy is the sum of the macroscopic energy and the microscopic correction energy. For high-energy fission, quantal effects are washed out. It implies that the microscopic effects have disappeared, such as the shell correction energy and the pairing correction. Under the assumption of nucleus volume conservation, for macroscopic energy, only the nuclear surface energy E_n and Coulomb energy E_C change during fission. By setting the potential origin to the spherical nuclear potential, the potential energy can be calculated as

$$V = E_n - E_{n0} + E_C - E_{C0}. \tag{9}$$

The macroscopic potentials are calculated with the finite range liquid drop model (FRLDM). The nuclear surface and Coulomb energy can be written in triple integral form as [31,32]

$$\begin{aligned} E_n = {} & \frac{a_S(1-k_S I^2)}{4\pi r_0^2} \iiint \left\{2 - \left[\left(\tfrac{\sigma}{a}\right)^2 + 2\tfrac{\sigma}{a} + 2\right]e^{-\sigma/a}\right\} \rho_s(z)\left[\rho_s(z) - \rho_s(z')\cos\phi - \frac{d\rho_s(z)}{dz}(z-z')\right] \\ & \times \rho_s(z')\left[\rho_s(z') - \rho_s(z)\cos\phi - \frac{d\rho_s(z')}{dz'}(z'-z)\right]\frac{dz dz' d\phi}{\sigma^4}, \end{aligned} \tag{10}$$

$$\begin{aligned} E_C = {} & \pi\rho_0^2 \iiint \left\{\frac{\sigma^3}{6} - a_d^3\left[2\frac{\sigma}{a_d} - 5 + \left(5 + 3\frac{\sigma}{a_d} + \frac{1}{2}\left(\frac{\sigma}{a_d}\right)^2\right)e^{-\sigma/a_d}\right]\right\}\rho_s(z)\left[\rho_s(z) - \rho_s(z')\cos\phi - \frac{d\rho_s(z)}{dz}(z-z')\right] \\ & \times \rho_s(z')\left[\rho_s(z') - \rho_s(z)\cos\phi - \frac{d\rho_s(z')}{dz'}(z'-z)\right]\frac{dz dz' d\phi}{\sigma^4}. \end{aligned} \tag{11}$$

The integration domain is the full space. Using the conversion relation between Cartesian and cylindrical coordinate systems, we can derive the expression of σ,

$$\begin{aligned} \sigma = {} & [\rho_s^2(z) + \rho_s^2(z') - 2\rho_s(z)\rho_s(z')\cos\phi \\ & + z^2 + z'^2 - 2zz']^{1/2}. \end{aligned} \tag{12}$$

The calculation results of potential energy surface for four deformation parameters $\eta = 0.2$, $\eta = 0.0$, $\delta = 0.2$, and $\delta = 0.0$ in $^{238}U(n, f)$ are shown in Fig. 2. The position of fission saddle point is also shown on the potential surface.

Initially, the momentum p_i is set to zero, the conservation forces (potential gradient) and random forces will drive the motion. For low energy fission, the Langevin trajectory often starts from the first potential saddle point or the first local minima, in order to increase the probability of getting available trajectory within a reasonable time and consume less computational resources to obtain statistical properties. However, at the excitation energy $E^* > 100$ MeV, considered in the present paper, the mean time from ground state to saddle point for heavy compound nuclei is about 10–100 zs [33], and there is only one saddle point on the potential surface. It is unreasonable to start from the first potential saddle point or the first local minima. Otherwise, the trajectory would lose the information of saddle point [34]. The problem of starting at the ground state ($z_0/R_0 = 0.0$) is that it sometimes leads to numerical calculation error because the ground state is at the boundary of potential space. Therefore, the starting point is chosen near the ground state ($z_0/R_0 = 0.5$) in the present work. The simulation result is not significantly sensitive to the choice of starting point [17,19,35]. Since the starting point of the trajectory is near the ground state and the ground state has a local minimum of potential energy, the trajectory is often trapped in this potential valley for long time or even moves out of the potential space during the Langevin calculation. For this reason, some artificial measures need to be applied to restrict the trajectory because we assume that the nucleus has decided to fission [36]. In order to reduce the trapped cases and keep the information of saddle point, the random force is restricted to be sign invariant in z_0/R_0 direction until a set value. In this work, the boundary of restriction is set as $z_0/R_0 = 1.7$, which is determined by comparing the data and the calculation. The value of starting point and restriction will be kept invariant for all cases shown in the present article.

The scission point is the end of one fission reaction, but the nucleus scission configuration is not fully understood. In the Langevin approach, the scission point is defined by the nucleus neck radius, and the neck radius setting value was found to have no significant effect on yield distribution [17]. So the criterion of the fission end is artificially set as the neck radius less than 0.5 fm.

D. Inertia and friction tensor

The inertia and friction tensors are calculated by the macroscopic model. By using the Werner-Wheeler approximation [37], the inertia tensor can be derived from the total kinetic energy and expressed as

$$m_{ij}(\boldsymbol{q}) = \pi\rho_m \int_{z_{\min}}^{z_{\max}} \rho_s^2(z, \boldsymbol{q})\left[A_i A_j + \frac{1}{8}\rho_s^2(z, \boldsymbol{q})A_i' A_j'\right]dz, \tag{13}$$

$$A_i = \frac{1}{\rho_s^2(z, \boldsymbol{q})}\frac{\partial}{\partial q_i}\int_z^{z_{\max}} \rho_s^2(z', \boldsymbol{q})dz', \tag{14}$$

where $\rho_m = 1.668 \times 10^{-45}$ MeV s^2 fm^{-5} is the nucleus density, A_i' is the derivative of A_i with respect to z.

The friction tensor is calculated by the macroscopic one-body wall-and-window model. By considering the nucleus surface as a wall, the energy dissipation of the collective motion comes from the collision between nucleons and the surface. For neckless nuclei, the wall dissipation is given as

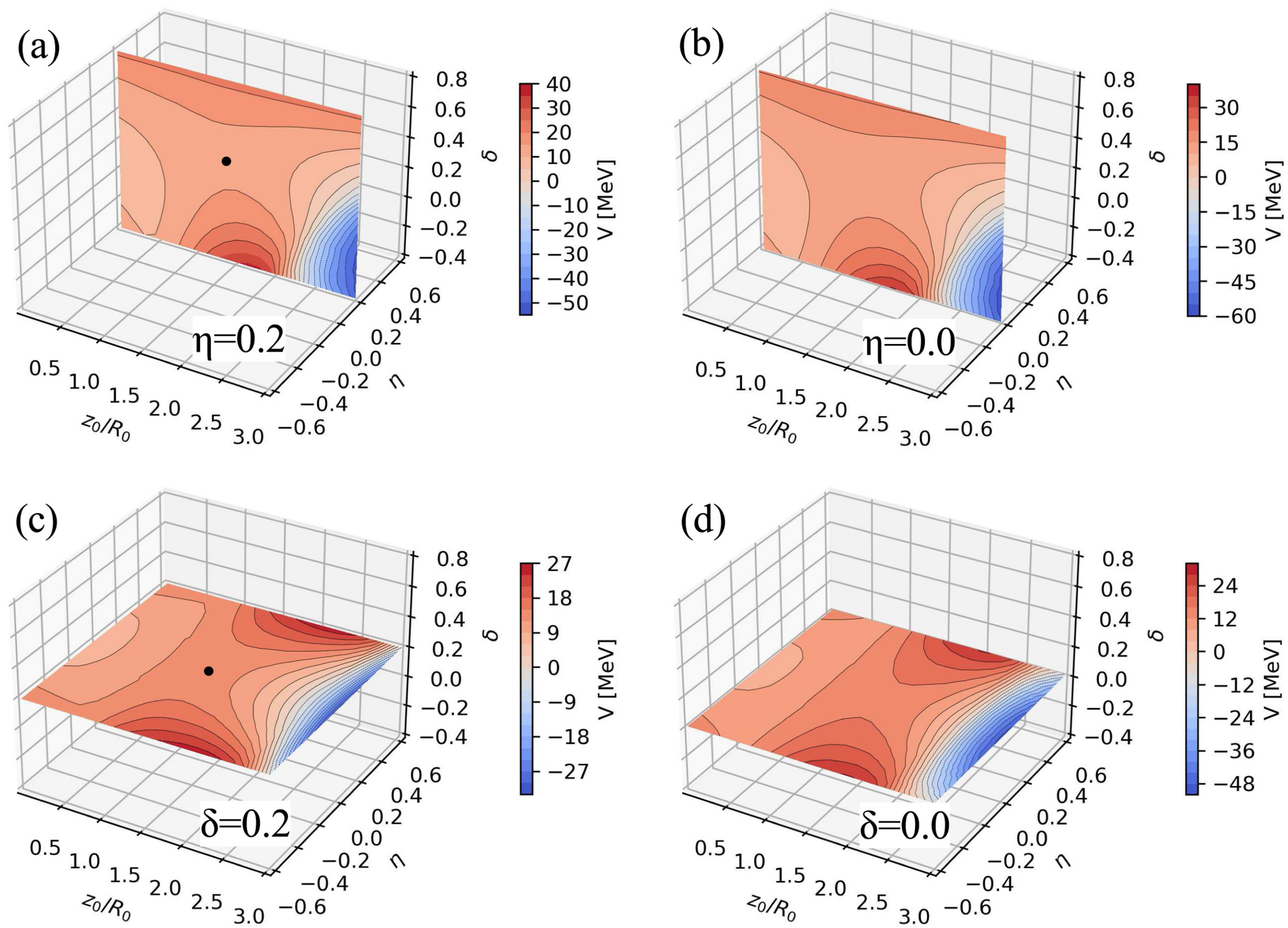

FIG. 2. Potential energy surface for four important deformation parameters in ^{238}U(n, f). Black dot represents the saddle point.

[38,39]

$$\gamma_{ij}^{\text{Wall}}(\boldsymbol{q}) = \frac{1}{2}\pi\rho_m\bar{v}\int_{z_{\min}}^{z_{\max}}\frac{\partial\rho_s^2}{\partial q_i}\frac{\partial\rho_s^2}{\partial q_j}\left[\rho_s^2+\frac{1}{4}\left(\frac{\partial\rho_s^2}{\partial z}\right)^2\right]^{-1/2}dz, \tag{15}$$

where $\bar{v} = 3v_f/4 \approx 6.4\times10^{22}$ fm/s is the average velocity of nucleons based on Fermi velocity. When the nucleus deforms and a neck has appeared, the nucleons in two pre-fragments exchange momentum with each other, showing the energy dissipation due to the neck. In this case, the friction tensor is calculated as [40]

$$\gamma_{ij}^{\text{W+W}}(\boldsymbol{q}) = \gamma_{ij}^{\text{Wall2}} + \gamma_{ij}^{\text{Window}} \tag{16}$$

with

$$\gamma_{ij}^{\text{Wall2}}(\boldsymbol{q}) = \frac{1}{2}\pi\rho_m\bar{v}\left(\int_{z_{\min}}^{z_N}I_L(z)dz + \int_{z_N}^{z_{\min}}I_R(z)dz\right), \tag{17}$$

$$I_v = \left(\frac{\partial\rho_s^2}{\partial q_i}+\frac{\partial\rho_s^2}{\partial z}\frac{\partial D_v}{\partial q_i}\right)\left(\frac{\partial\rho_s^2}{\partial q_j}+\frac{\partial\rho_s^2}{\partial z}\frac{\partial D_v}{\partial q_j}\right)\times\left[\rho_s^2+\frac{1}{4}\left(\frac{\partial\rho_s^2}{\partial z}\right)^2\right]^{-1/2}, \tag{18}$$

where $v = L, R$ represents the pre-fragments on the left and right sides of the neck, z_N is the position of the smallest neck radius, which equals 0 in the present work, D_v is the mass center position of two pre-fragments. The window dissipation is calculated as [41]

$$\gamma_{ij}^{\text{Window}}(\boldsymbol{q}) = \frac{1}{2}\rho_m\bar{v}\left(\frac{\partial R_{12}}{\partial q_i}\frac{\partial R_{12}}{\partial q_j}\Delta\sigma + \frac{32}{9\Delta\sigma}\frac{\partial V_R}{\partial q_i}\frac{\partial V_R}{\partial q_j}\right), \tag{19}$$

where R_{12} denotes the distance between the mass center of pre-fragments, $\Delta\sigma$ represents the window area, and V_R is the volume of right pre-fragment. Nix and Sierk proposed a phenomenological formula to smoothly transition this two friction [42]

$$\gamma_{ij} = \tau\left(\gamma_{ij}^{\text{W+W}}\right) + (1-\tau)\gamma_{ij}^{\text{Wall}}. \tag{20}$$

The choice of τ is subjective [43,44] and the present work used the expression in Ref. [42]

$$\tau = \cos^2\left(\frac{\pi}{2}\frac{r_N^2}{b_{\min}^2}\right), b_{\min} = \min(b_1, b_2), \tag{21}$$

where r_N is the neck radius.

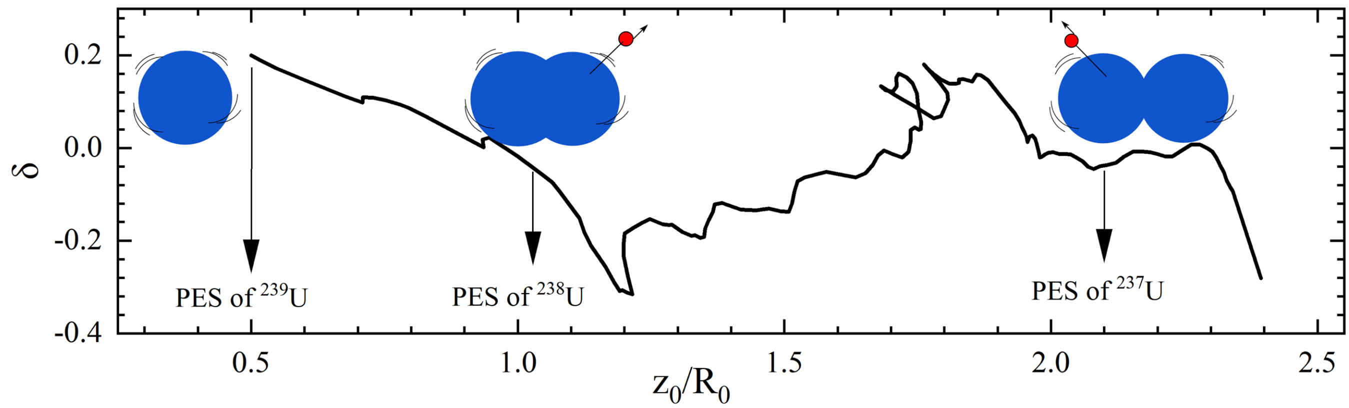

FIG. 3. Langevin trajectory for ^{238}U(n, f) projected on $z_0/R_0 - \delta$ plane. The change of potential energy space due to the pre-scission neutron emission during fission is also shown in the figure.

E. Pre-scission neutrons emission

The pre-scission neutron emission behavior is regarded as a nucleus decay process. According to the exponential decay law, the number of decayed particles N' in a initial N_0 particles system can be expressed as

$$N' = N_0(1 - \exp(-\Gamma t)). \tag{22}$$

Within time step Δt, the variation of particles number $\Delta N'$ can be approximately derived from the differential of N',

$$\Delta N' = \Delta t N_0 \Gamma \exp(-\Gamma t). \tag{23}$$

Then the probability P of a nucleus decay within one Langevin time step Δt is expressed as

$$P = \Delta N'/N_0 = \Delta t \Gamma \mathrm{e}^{-\Gamma t}. \tag{24}$$

During the simulation, one emission event is allowed by checking at each time step whether P is larger than a random number ranging from 0 to 1 [36]. Once a neutron emission has occurred, the Langevin trajectory will be converted to the potential energy space (PES) of the corresponding compound nucleus, as shown in Fig. 3. In Eq. (24), Γ is the decay width calculated by the Hauser-Feshbach statistical decay model. For a fissile system (Z_0, A_0) with excitation energy E^* and spin S_{CN}, if a light particle (Z_i, A_i) with spin S_i is emitted and leaves a residual system (A_d, Z_d) with spin S_d, then the decay width can be expressed as [45]

$$\Gamma^{\mathrm{HF}} = \frac{1}{2\pi \rho_0} \int d\varepsilon \sum_{S_d=0}^{\infty} \sum_{J=|S_{CN}-S_d|}^{S_{CN}+S_d} \sum_{l=|J-S_i|}^{J+S_i} T_l(\varepsilon)\rho(U, S_d), \tag{25}$$

where ϵ, J, and l are the kinetic energy, spin, and orbit angular momentum of the emitted particle, ρ_0 and $\rho(U, S_d)$ are the level densities of the initial and residual systems, respectively, T_l is the transmission coefficient. The thermal excitation energy U is written as $U = E^* - B_{\mathrm{pre}} - \epsilon$ with the excitation energy E^* and the separation energy B_{pre}. The transmission coefficients are calculated from the inverse reaction using the optical model parameters obtained from global optical-model fits to elastic scattering data. The level density of residual spherical nucleus are calculated by Fermi gas model [46]

$$\rho(E^*, J) \propto \frac{(2J+1)\exp[2\sqrt{a(E^* - E_1)}]}{a^{1/4}[1 + (E^* - E_1)^{5/4}]}. \tag{26}$$

In the level density calculations, the nucleus deformation during fission is not considered. Reference [2] has discussed the effect of deformation on the pre-scission neutron emission based on a one-dimensional Langevin approach.

III. RESULTS AND DISCUSSION

A. Excitation energy dependence of pre-scission neutron emission

This section investigates the energy dependence of the emitted neutron multiplicity and the neutron kinetic energy spectrum before the scission point. Neutron-induced ^{238}U fission reactions are simulated at three energies: 110, 325, and 500 MeV. Figure 4 shows the occurrence probability of the fission event with different pre-scission neutron multiplicity. It is shown that the percentages of the fission events without neutron emission are 36%, 31%, and 28%. In other words, about 70% fission events in the studied energy region incur neutron emission before the scission point. The percentages of the fission events decrease with increasing neutron multiplicity, and are less than 5% for emitting five neutrons. Emission numbers over 5 are not shown in the figure, but their percentages are considerable, about 8%. The average multiplicities of the neutrons are 1.43, 1.88, 2.16 in ^{238}U(n, f) fission at 110, 325, and 500 MeV, respectively. As the incident energy increases, the average multiplicity also increases. In a single fission event, the probability of multiple neutrons emission increases and the probability of no or one emitted neutron event decreases. It corresponds to the fact that the higher excitation energy system has the larger decay width and then greater probability of decay.

Figure 5 shows the kinetic energy spectra of the neutrons emitted before the scission point. The spectra are in the form of a single peak with trailing in the high-energy region. The peak position shows that most of the neutron kinetic energies

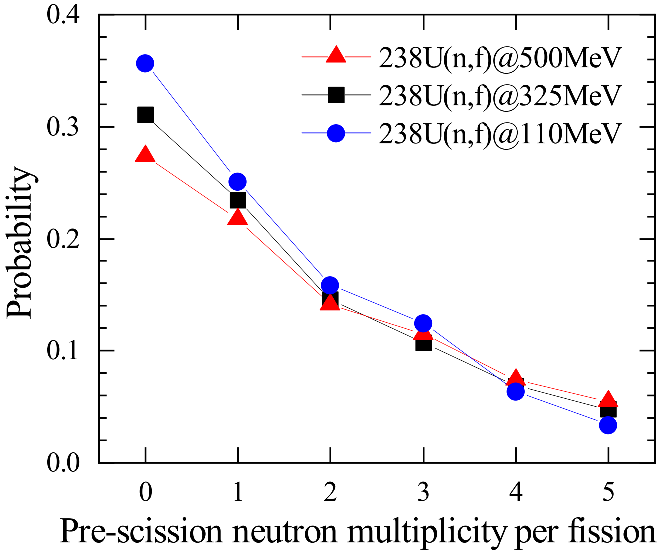

FIG. 4. The calculated pre-scission neutron multiplicity per fission in ^{238}U(n, f) at 110, 325, and 500 MeV induced energy.

are below 10 MeV for all cases. As the excitation energy increases, the peak position moves to the high energy region and the peak height decreases. The average kinetic energies of the neutrons are 3.89, 7.77, 9.93 MeV for ^{238}U(n, f) fission at 110, 325, and 500 MeV, respectively. The increase of the kinetic energy of the emitted neutrons reduces more excitation energy of the compound nucleus. The simulated value indicates that the energy carried away by neutron emission cannot be neglected. This leads to an excitation energy decrease of the nascent fragments, which would affect the calculation of prompt and delayed neutrons. In general, more energy is carried away from the highly excited compound nucleus by emitting higher kinetic energies and a larger number of neutrons.

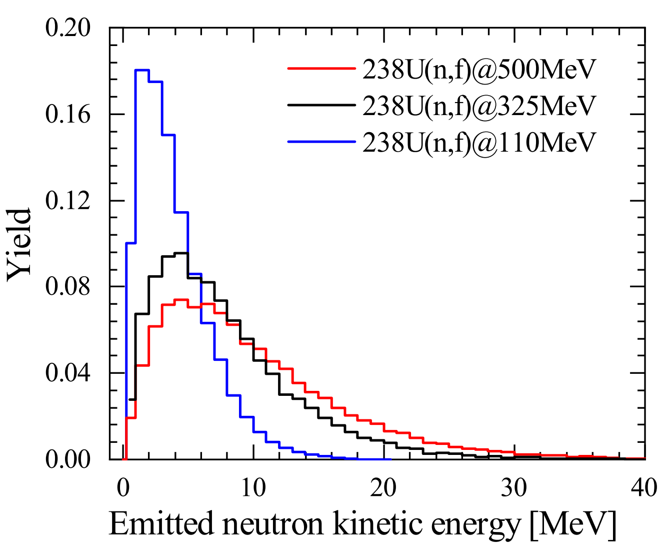

FIG. 5. The calculated pre-scission neutron kinetic energy in ^{238}U(n, f) at 110, 325, and 500 MeV induced energy.

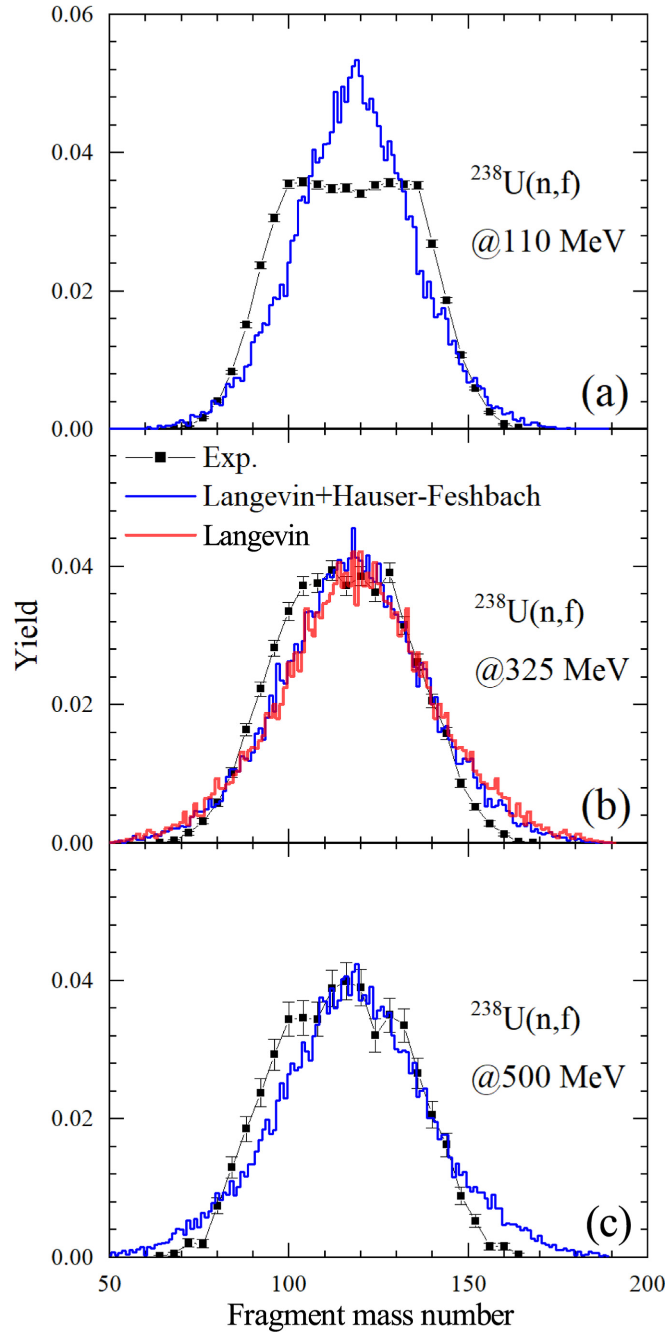

FIG. 6. The calculated fragment mass distributions in 110, 325, 500 MeV ^{238}U(n, f) compared with the experimental data [16].

B. Pre-scission neutron emission influence on fragment mass distribution, total kinetic energy distribution, and scission-point deformation

This section investigates the influence of pre-scission neutron emission on the fragments mass, total kinetic energy (TKE), and deformation distribution. With and without account of the pre-scission neutron emission, the fragment mass distribution at 110, 325, 500 MeV, the TKE distribution and the deformation distribution at 325 MeV in the ^{238}U(n, f) reaction are shown in Figs. 6–8, respectively.

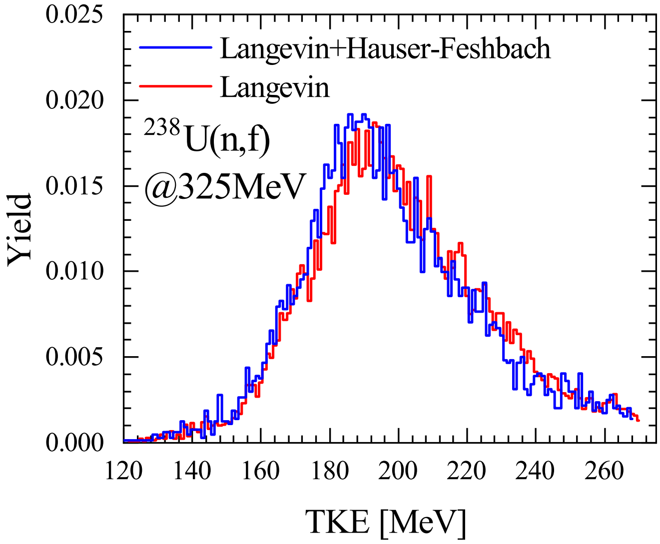

FIG. 7. The calculated total kinetic energy of fission fragments in 325 MeV ^{238}U(n, f).

Table I shows the comparison between the simulated and experimental data of average fragment mass at three induced neutron energies. The difference between experimental data and column "Langevin" shows the contribution of the emission to the fragments average mass reduction phenomenon. The higher excitation energy causes the higher decrease in the average mass of the fragments. This similar excitation energy dependence of fragment mass reduction and pre-scission neutron multiplicity demonstrates a strong correlation between the two. However, the calculations with the Hauser-Feshbach decay model is still larger than experimental data. It is due to the fact that for high-energy neutron-induced fission, a certain number of neutrons emit during the pre-equilibrium

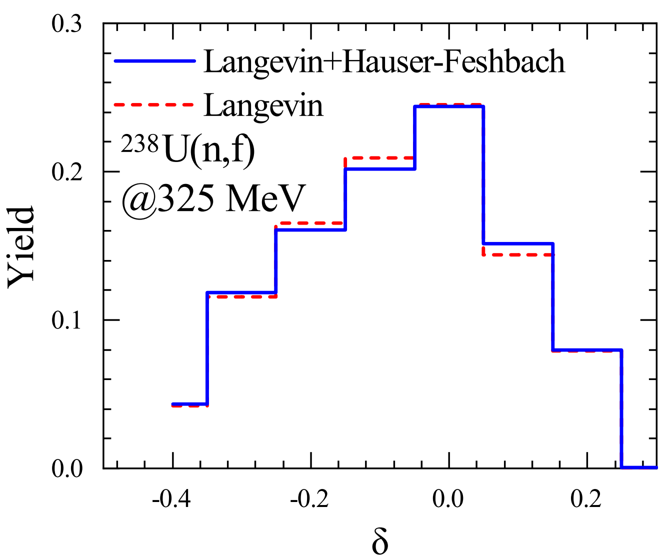

FIG. 8. The calculated fragment deformation distribution in 325 MeV ^{238}U(n, f) compared with the one without considering neutron emission.

TABLE I. Experimental data and calculations of average fragment mass in ^{238}U(n, f).

Induced energy [MeV]	Exp.[a]	Langevin	Langevin +Hauser-Feshbach
110	117.4	119.5	118.3
325	116.0	119.5	118.0
500	115.1	119.5	117.9

[a]Experimental data are taken from [16].

phase. The current Langevin method considers the compound nucleus assumption, which does not take into account the stage of neutron incidence to the statistical equilibrium of the system, so the fragment mass reduction is underestimated. It is also partly related to the restriction on the random force when the nucleus is near the ground state. This restriction leads to a smaller fission time prediction and then a smaller emitted neutron number in a single fission event, but the tendency is preserved.

Figure 6 shows the fragment mass distribution in ^{238}U(n, f) fission at 110, 325, 500 MeV. At 110 MeV, the symmetric fission yield is overestimated. The possible explanation of the discrepancy between theory and experimental data could be the multichance fission mechanism [47,48]. Since the pre-scission neutron emission will cause the energy reduction of the compound nucleus, the combination of the single-peak distribution at higher excitation energy and the double-peak distribution at lower excitation energy leads to the wider maximum distribution. For the reason that the shell effect is not involved in the present work, the experimental wider maximum was not reproduced. For 325 MeV incident energy, the simulation results has better agreement with the experimental values. The yields of $A > 150$ fragments are slightly overestimated and the yield around $A = 100$ is underestimated. The comparison between the calculations with and without an account of neutron emission shows that the fragments mass reduction is represented as a leftward shift of peak position, which is in agreement with the trends in experimental data. For 500 MeV incident energy, the simulation results reproduce the symmetric fission yield well, but overestimate the fission fragment yield for $A < 80$ and $A > 150$. This overestimation indicates that higher excitation energy leads to higher random force strength, and then to a wider wandering area of Langevin motion near the scission point.

In the investigation of the influence of pre-scission neutron emission on the TKE distribution, the TKE of fragments is calculated as [49]

$$\mathrm{TKE} = V_{\mathrm{Coul}} + E_{\mathrm{kin}}, \tag{27}$$

where $V_{\mathrm{Coul}} = Z_1 Z_2 e^2/D$ and $E_{\mathrm{kin}} = 1\backslash 2(m^{-1})_{ij} p_i p_j$ are the Coulomb repulsion energy of point charge of fragments and the kinetic energy at scission point. Coulomb repulsive energy is the dominant one. Figure 7 shows a leftward shift of the total kinetic energy distribution lead by pre-scission neutron emission. It indicates that the emitted neutrons carry away part of the fragments TKE. The average TKE also shows this reduction. Without and with considering the neutron emission, $\langle$TKE$\rangle$ equals to 200.57 MeV and 198.65 MeV, respectively.

Figure 8 shows the calculations of the fragment deformation yield with and without taking into account the pre-scission neutron emission. About 75% of the fission fragments have $\delta \leqslant 0$, indicating that fragments tends to form in spherical or prolate ellipsoid shape. The prolate ellipsoid fragments will cause a higher kinetic energy. The comparison shows that neutron emission has no significant influence on the deformation distribution. The reason is that the change of potential energy in δ direction is not significant between different uranium isotope. And the gentler saddle point structure in Fig. 2 also reduces the influence of potential energy gradient on the fission trajectory.

IV. SUMMARY

In this work, the Langevin approach is developed by combining the three-dimensional Langevin fission dynamics approach with the Hauser-Feshbach statistical decay model. Three collective variables are used to describe the nucleus shape, which are the nucleus elongation, fragment mass asymmetry, and nucleus deformation. The decay width of neutron emission is calculated by the Hauser-Feshbach model. Based on this developed Langevin approach, the influence of the pre-scission neutron emission on the high-energy neutron induced ^{238}U fission is studied.

The multiplicity and the kinetic energy of the pre-scission emitted neutrons are first investigated. It is shown that the average multiplicities of the neutrons are 1.43, 1.88, 2.16, and the average kinetic energies of the neutrons are 3.89, 7.77, 9.93 MeV for ^{238}U(n, f) fission at 110, 325, 500 MeV, respectively. The pre-scission emitted neutrons result in substantial reduction of the mass and excitation energy of the fissioning system. The influences of pre-scission neutron emission on the mass distribution, total kinetic energy distribution, and deformation distribution of fission fragments are then investigated. For the fragments mass, it is shown that the experimentally observed average mass loss of fragments can be partially reproduced after taking into account the pre-scission neutron emission. The discrepancy between the simulated and experimental values of average mass in this work probably comes from the pre-equilibration stage before the compound nucleus formation. For the independent and cumulative yield, post scission particles emission also needs to be considered. The effect of multichance fission on the shape of mass yield is significant, especially for the 110 MeV case. By the multichance fission mechanism, the mass distribution at 110 MeV is the combination of the symmetry fission mass distribution and the asymmetry one. For the total kinetic energy of the fragments, the pre-scission neutron emission similarly leads to a leftward shift of the distribution by about 2 MeV. The calculations of the deformation yield show that about 75% of the fragments are produced in spherical and prolate ellipsoid shape. This distribution arises from the gentle potential energy configuration at saddle point in the ^{238}U(n, f) reaction. In addition, the influence of pre-scission neutron emission on the deformation yield is weak.

Further improvements of the model are needed in future work. First, proton and α particle emission will be considered. It requires the use of a decay width database containing more kinds of particles, and a potential energy surface database containing more kinds of compound nuclei to cover all different combinations of particle emission. Second, the particle emission in the pre-equilibrium stage will be considered. The distribution of initial state mass number and excitation energy should be considered instead of the single value. Third, the effect of deformation on the level density in the decay width calculation will be considered. The current calculations are based on the spherical nucleus.

ACKNOWLEDGMENTS

The authors would like to thank Dr. L.-L. Liu for helpful discussion and suggestions.

[1] R. Sandal, B. R. Behera, V. Singh, M. Kaur, A. Kumar, G. Singh, K. P. Singh, P. Sugathan, A. Jhingan, K. S. Golda *et al.*, Phys. Rev. C **87**, 014604 (2013).
[2] N. Kumar, S. Mohsina, J. Sadhukhan, and S. Verma, Phys. Rev. C **96**, 034614 (2017).
[3] J. Sadhukhan and S. Pal, Phys. Rev. C **78**, 011603(R) (2008).
[4] J. Sadhukhan and S. Pal, Phys. Rev. C **81**, 031602(R) (2010).
[5] V. Singh, B. R. Behera, M. Kaur, A. Kumar, P. Sugathan, K. S. Golda, A. Jhingan, M. B. Chatterjee, R. K. Bhowmik, D. Siwal *et al.*, Phys. Rev. C **87**, 064601 (2013).
[6] W. Ye, Phys. Rev. C **79**, 031601(R) (2009).
[7] N. Wang and W. Ye, Phys. Rev. C **87**, 051601(R) (2013).
[8] Y. Aritomo, M. Ohta, T. Materna, F. Hanappe, O. Dorvaux, and L. Stuttge, Nucl. Phys. A **759**, 309 (2005).
[9] D. J. Hinde, D. Hilscher, H. Rossner, B. Gebauer, M. Lehmann, and M. Wilpert, Phys. Rev. C **45**, 1229 (1992).
[10] D. Hilscher, H. Rossner, B. Cramer, B. Gebauer, U. Jahnke, M. Lehmann, E. Schwinn, M. Wilpert, T. Wilpert, H. Frobeen *et al.*, Phys. Rev. Lett. **62**, 1099 (1989).
[11] D. Hinde, D. Hilscher, and H. Rossner, Nucl. Phys. A **502**, 497 (1989).
[12] P. Roy, K. Banerjee, C. Bhattacharya, R. Pandey, A. Sen, S. Manna, S. Kundu, T. K. Rana, T. K. Ghosh, G. Mukherjee *et al.*, Phys. Rev. C **94**, 064607 (2016).
[13] K. Banerjee, S. Bhattacharya, C. Bhattacharya, M. Gohil, S. Kundu, T. K. Rana, G. Mukherjee, R. Pandey, P. Roy, H. Pai *et al.*, Phys. Rev. C **85**, 064310 (2012).
[14] D. Mondal, D. Pandit, S. Mukhopadhyay, S. Pal, B. Dey, S. Bhattacharya, A. De, S. Bhattacharya, S. Bhattacharyya, P. Roy *et al.*, Phys. Rev. Lett. **118**, 192501 (2017).
[15] D. Hinde, Nucl. Phys. A **553**, 255 (1993).
[16] C. M. Zöller, Investigation of the neutron-induced fission of ^{238}U in the energy range 1 MeV to 500 MeV, Ph.D. thesis, Department of Physics, Technische Hochschule Darmstadt, 1995.
[17] L.-L. Liu, X.-Z. Wu, Y.-J. Chen, C.-W. Shen, Z.-X. Li, and Z.-G. Ge, Phys. Rev. C **99**, 044614 (2019).
[18] K. H. Schmidt and B. Jurado, Rep. Prog. Phys. **81**, 106301 (2018).

[19] M. D. Usang, F. A. Ivanyuk, C. Ishizuka, and S. Chiba, Phys. Rev. C **94**, 044602 (2016).
[20] F. Ivanyuk, S. Chiba, and Y. Aritomo, J. Nucl. Sci. Technol. **53**, 737 (2016).
[21] J. Sadhukhan, W. Nazarewicz, and N. Schunck, Phys. Rev. C **93**, 011304(R) (2016).
[22] Y. Wei, W. Feng, and Y. Hong-Wei, Chin. Phys. C **32**, 816 (2008).
[23] H. Eslamizadeh, Eur. Phys. J. A **47**, 134 (2011).
[24] D. Naderi, S. A. Alavi, and V. Dehghani, Int. J. Mod. Phys. E **28**, 1950077 (2019).
[25] M. R. Pahlavani and D. Naderi, Phys. Rev. C **83**, 024602 (2011).
[26] Y. Jia and J.-D. Bao, Phys. Rev. C **75**, 034601 (2007).
[27] J. Maruhn and W. Greiner, Z. Phys. **251**, 431 (1972).
[28] S. Yamaji, H. Hofmann, and R. Samhammer, Nucl. Phys. A **475**, 487 (1987).
[29] H. Hofmann and D. Kiderlen, Int. J. Mod. Phys. E **07**, 243 (1998).
[30] M. D. Usang, F. A. Ivanyuk, C. Ishizuka, and S. Chiba, Phys. Rev. C **96**, 064617 (2017).
[31] H. J. Krappe, J. R. Nix, and A. J. Sierk, Phys. Rev. C **20**, 992 (1979).
[32] K. T. R. Davies and J. R. Nix, Phys. Rev. C **14**, 1977 (1976).
[33] P. N. Nadtochy, E. G. Ryabov, A. E. Gegechkori, Y. A. Anischenko, and G. D. Adeev, Phys. Rev. C **89**, 014616 (2014).
[34] C. Ishizuka, M. D. Usang, F. A. Ivanyuk, J. A. Maruhn, K. Nishio, and S. Chiba, Phys. Rev. C **96**, 064616 (2017).
[35] A. J. Sierk, Phys. Rev. C **96**, 034603 (2017).
[36] N. D. Mavlitov, P. Fröbrich, and I. I. Gonchar, Z. Phys. A **342**, 195 (1992).
[37] K. T. R. Davies, A. J. Sierk, and J. R. Nix, Phys. Rev. C **13**, 2385 (1976).
[38] J. Blocki, Y. Boneh, J. Nix, J. Randrup, M. Robel, A. Sierk, and W. Swiatecki, Ann. Phys. (NY) **113**, 330 (1978).
[39] A. J. Sierk and J. R. Nix, Phys. Rev. C **21**, 982 (1980).
[40] G. D. Adeev, A. V. Karpov, P. N. Nadtochy, and D. V. Vanin, Phys. Part. Nucl. **36**, 378 (2005).
[41] W. J. Swiatecki, Nucl. Phys. A **428**, 199 (1984).
[42] J. Rayford Nix and A. J. Sierk, Nucl. Phys. A **428**, 161 (1984).
[43] J. Bžocki, J. Phys. Colloques **45**, 489 (1984).
[44] H. Feldmeier, Rep. Prog. Phys. **50**, 915 (1987).
[45] W. Hauser and H. Feshbach, Phys. Rev. **87**, 366 (1952).
[46] J. Su, L. Zhu, and C. Guo, Phys. Rev. C **97**, 054604 (2018).
[47] C. Schmitt, K.-H. Schmidt, and B. Jurado, Phys. Rev. C **98**, 044605 (2018).
[48] K. Hirose, K. Nishio, S. Tanaka, R. Léguillon, H. Makii, I. Nishinaka, R. Orlandi, K. Tsukada, J. Smallcombe, M. J. Vermeulen *et al.*, Phys. Rev. Lett. **119**, 222501 (2017).
[49] Y. Aritomo, S. Chiba, and F. Ivanyuk, Phys. Rev. C **90**, 054609 (2014).